

2021-12

Suitability of bio-desiccants for energy wheels in HVAC applications

Alabi, Wahab O

Elsevier

Wahab O. Alabi, Easwaran N. Krishnan, Abdalla H. Karoyo, Leila Dehabadi, Lee D. Wilson, Carey J. Simonson, Suitability of bio-desiccants for energy wheels in HVAC applications, *Building and Environment*, (206), 2021, 108369. <https://doi.org/10.1016/j.buildenv.2021.108369>
<https://hdl.handle.net/10388/14796>

Downloaded from HARVEST, University of Saskatchewan's Repository for Research

1 **SUITABILITY OF BIO-DESICCANTS FOR ENERGY WHEELS IN HVAC**
2 **APPLICATIONS**

3 Wahab O. Alabi¹, Easwaran N. Krishnan^{1*}, Abdalla H. Karoyo², Leila Dehabadi², Lee D.
4 Wilson², Carey J. Simonson¹

5 ¹Department of Mechanical Engineering, University of Saskatchewan, 57 Campus Drive,
6 Saskatoon, SK S7N 5A9, Canada

7 ²Department of Chemistry, University of Saskatchewan, 110 Science Place, Saskatoon,
8 SK S7N 5C9, Canada

9
10 **ABSTRACT**

11 This paper investigates the suitability of bio-desiccants for moisture recovery in energy
12 wheels. Bio-desiccants are environment-friendly materials that have high water vapor adsorption
13 capacities. The main contribution of this paper is that it reports the latent effectiveness of flax-
14 fiber (bio-desiccant) coated energy wheels for a wide range of operating conditions and compares
15 the effectiveness of the flax-fiber wheels with wheels that are coated with commercially available
16 desiccants and ~~some~~ other biomaterials. The moisture transfer performance of a flax-fiber coated
17 exchanger is determined using a small-scale test facility and two different experimental methods:
18 single step change tests and cyclic tests. The test results are used to verify the applicability of an
19 effectiveness correlation from the literature. Using the energy wheel correlation and the sorption
20 isotherms, the latent effectiveness of commercially available energy wheels coated with molecular
21 sieve, ion exchange resin and silica gel desiccants are obtained and compared with that of bio-
22 desiccants (flax fiber and starch particles). The highest latent effectiveness is obtained for silica
23 gel followed by starch particles, ion exchange resin, flax-fiber and molecular sieve. The results
24 from this study will be useful in research and development of bio-materials for energy recovery
25 systems for building applications.

26 **Keywords:** flax-fiber, adsorption, desorption, latent effectiveness, bio-desiccants.

*corresponding author: Easwaran N. Krishnan: enk133@mail.usask.ca

Nomenclature

A_s	total heat transfer area(m^2)
Cr^*	matrix heat capacity rate ratio
Cr_m^*	matrix moisture capacity rate ratio
h	convective heat transfer coefficient ($W\ m^{-2}K^{-1}$)
H^*	operating condition factor
M	mass of the exchanger (kg)
M_d	mass fraction of desiccant
\dot{m}	mass flow rate of air ($kg\ s^{-1}$)
NTU	number of transfer units
P/P_0	relative pressure
Q_a	volume flow rate ($L\ min^{-1}$)
Re_{ch}	channel Reynolds number
T	temperature ($^{\circ}C$)
t	time (s)
U	overall uncertainty
V_f	face velocity ($m\ s^{-1}$)
W	humidity ratio ($g\ g^{-1}$)
W_m	maximum moisture uptake ($g_w\ g_d^{-1}$)

Abbreviations

CF	counter flow
AAEE	air-to-air energy exchanger
DEM	double exponential model
FF	flax-fiber
IAQ	indoor air quality
HVAC	heating ventilation and air-conditioning
PF	parallel flow

Greek Symbols

ε_l	latent effectiveness (%)
Φ	relative humidity (%)
τ	time constant (s)
ω	rotational speed (rpm)

Subscripts

ads	adsorption
ave	average
des	desorption
s	surface

1

2 1. INTRODUCTION

3 The role of indoor air quality (IAQ) has been related to the health and comfort of its
4 occupants [1]. With an estimation that people spend 90 % of their time indoors [1], good IAQ can
5 contribute to the productivity, comfort, physical and mental health of occupants of the buildings
6 [2]. The level of IAQ and thermal comfort depends mainly on the humidity, temperature, and the
7 ventilation rate of air within the environment, which are regulated by the heating, ventilation, and
8 air condition (HVAC) systems [3]. The achievement of a standard IAQ level in buildings along
9 with other operations involves the use of energy, where it has been estimated that HVAC systems

1 consume 65% of the energy in buildings [4]. With a projected exponential increase in energy
2 consumption over the century due to climate change and other energy needs, there is a need to
3 develop energy efficient and cost-effective HVAC systems.

4 HVAC systems furnished with air-to-air energy exchangers (AAEEs) reduce the energy
5 consumption as compared to conventional HVAC systems [5,6]. Energy wheels are the most
6 common AAEEs used in commercial buildings, which are designed to transfer both heat and
7 moisture between the supply and exhaust air streams. During the past decades, extensive research
8 has been done to model the heat and moisture transfer process in energy wheels and it is found that
9 the latent effectiveness depends on sorption properties of the materials [7–10]. Few correlations
10 are also developed for the effectiveness evaluation. However, these have limited validity as the
11 nature of materials significantly influence the performance, type of desiccant coating, matrix
12 thermal and physical properties, and operating conditions [8,11,12].

13 On the other hand, experiments on full-scale exchangers are also challenging because of
14 the high cost per test, requirement of full-scale exchangers (important during product
15 development), large ducting size, and the high volume of conditioned airflow [13–16]. HVAC
16 engineers and manufacturers are interested in alternate test methods to overcome the challenges in
17 full-scale testing. Abe et al. [13] have developed a new method called transient testing (or single-
18 step change test) for performance evaluation of rotary wheels. In this method, effectiveness of a
19 wheel is predicted from its transient response to a step-change in inlet conditions (temperature or
20 humidity). Later on, and Fathieh et al. [11,17] showed that the performance of the wheel could be
21 predicted by testing a similar small-scale heat exchanger. This method is validated with a
22 numerical model and literature correlations that are later applied for evaluating the performance
23 of energy wheels with various desiccant materials [13,18–22].

24 Various studies have reported the utility of silica gel [23,24] zeolites [12,25] metal-organic
25 frameworks [26,27] and activated alumina [28,29] as desiccant coatings in heat exchangers or
26 wheels. The main differences between desiccant coated exchangers (DCHE or desiccant wheels)
27 from conventional energy wheels is need for a dedicated section for regeneration for DCHE, which
28 typically requires a heat source. In general, the DCHE contains a multilayer of desiccants to
29 exchange maximum water vapor, which could reduce the heat transfer effectiveness. However,
30 energy wheels are passive devices where the simultaneous heat and moisture transfer occur due to

1 the temperature and humidity difference between the return and supply airstreams. The
2 dehumidification performance of a silica gel and polyvinyl alcohol-LiCl heat exchanger was
3 previously reported [30], where the maximum coefficient of performance (COP) was reported as
4 0.15 and 0.33, respectively. Li et al. [31] studied the heat and mass transfer performance of a
5 desiccant-coated fin tube exchanger. They found that the air velocity, temperature, and moisture
6 content of desiccant affects the overall mass transfer coefficients. Recently, Wang et al. [32]
7 presented the operation and performance of a desiccant-coated microchannel heat exchanger
8 (MCHE). Compared to conventional DCHEs, MCHEs are lightweight with a high heat transfer
9 coefficient that requires small volume.

10 Since most investigations on desiccant-coated exchangers are based on conventional
11 materials, the handling, treatment, and disposal of these synthetic materials can be a concern during
12 their industrial-scale manufacture. The use of biomass-derived materials could address some of
13 these sustainability concerns as they are known to possess good water sorption properties, high
14 abundance, and relatively low cost [33–35]. Improved moisture performance has been reported for
15 bio-materials such as starch particles (SP) from the “Prairie Carnation” (*Saponaria vaccaria*)
16 flower [22] and high amylose starch (HAS) [36], which were compared with silica gel (SG) coated
17 energy wheels. Although the sorption properties of biomaterials under dynamic flow conditions
18 are favorable, their durability over several sorption cycles and time, under different temperature
19 and humidity conditions, is a major concern for large scale industrial usage [11,37]. Thus, other
20 biomaterials (such as flax-fiber, wheat straw, cassava) could be valuable as potential desiccants
21 for moisture uptake in energy wheel, as FF was recently reported as a potential desiccant for energy
22 wheel application [21,38,39].

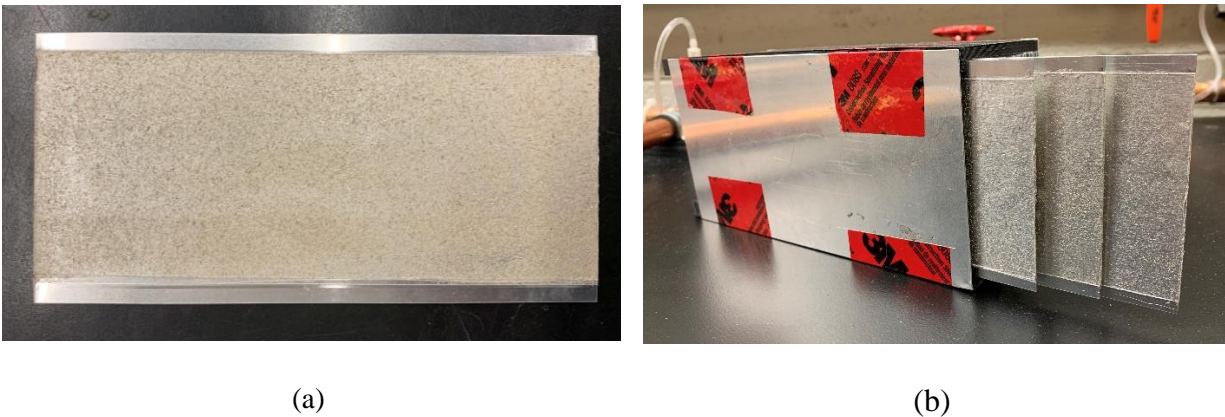
23 To extend our research contribution in the area of bio-desiccants, the sorption performance
24 of FF as a potential desiccant for an energy wheel under wide range of test conditions is presented
25 in this paper. Although the characterization of the hydration and water vapor uptake properties of
26 the FF material has been reported previously [38], a study on the sorption kinetics based on the
27 moisture recovery of the desiccants in energy wheel applications is provided herein. The major
28 objectives of this present work include the following: (1) To study the effect of the desiccant mass
29 fraction on the sorption performance of FF coated energy wheels using both single-step change
30 and cyclic methods, (2) To use the experimental results to validate literature correlation of latent

1 effectiveness, and (3) To use literature correlations to compare the latent effectiveness of
 2 commercially available desiccants and biomaterials for energy wheel applications.

3 **2. EXPERIMENTAL SECTION**

4 **2.1 Flax-fiber (FF) coated Parallel-Plate Exchanger.**

5 Rectangular aluminum plates (Al) with the dimensions 20 cm × 9 cm × 0.65 mm were cut
 6 from Al-3003 sheets purchased from McMaster-Carr, USA. The FF desiccant (particle size ≈210
 7 μm) was coated onto the Al-sheets (cf. Fig. 1(a)) using the sieving method developed by Hossain
 8 et al. [36], Subsequently, a small-scale parallel plate exchanger (20cm × 10cm × 7cm) was
 9 assembled using 16 Al-sheets coated with FF (Fig. 1(b)), and the other design details of the FF
 10 coated small-scale exchanger are listed in Table 1.



11 **Figure 1.** Photograph images: (a) flax-fiber (FF)-coated aluminum plate, and (b) small-scale
 12 energy exchanger.

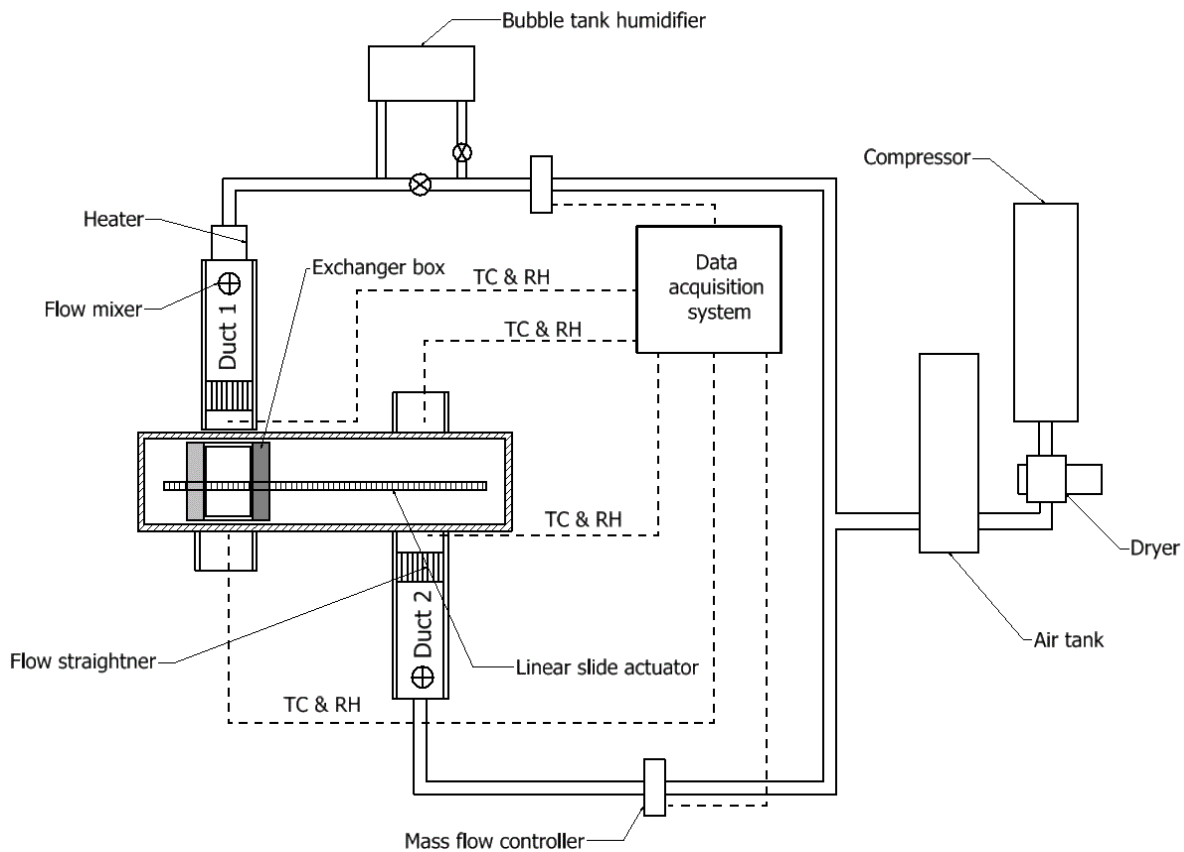
13 **Table 1:** Mass of flax-fiber desiccant coated on a small-scale exchanger

Desiccant	Mass of Coating (g)	Desiccant mass/coated area (mg/cm ²)	Desiccant/Matrix mass ratio (%)	Mass fraction of desiccant (M _d)
Flax-fiber	11.6 ± 0.02	2.44 ± 0.005	2.33	0.023

14
 15 **2.2 Test Apparatus and Experimental Procedure**

16 A schematic diagram of the recently modified test facility is shown in Fig. 2. It consists of
 17 two units, an air stream pre-conditioning section, and the test section. The pre-conditioning unit is

1 comprised of a supply air system, where a compressor is in line with a dehumidifier. The air
 2 streams are conditioned using a humidifier, mass flow controllers, and heaters. The temperature
 3 and relative humidity (RH) of the air stream can be easily varied to simulate different operating
 4 conditions. In the test unit, air ducts 1 and 2 serve as inlet streams to the test exchanger that are
 5 used for air supply to the exchanger in a counter-flow direction. Flow straighteners are also placed
 6 in each airstream before the exchanger inlet, to provide a uniform velocity profile at the exchanger
 7 inlet.



8

9 **Figure 2.** Schematic diagram of the energy wheel test facility.

10 Five thermocouples (upstream), nine thermocouples (downstream), and four RH sensors (in each
 11 outlet duct) are placed around the exchanger to measure the temperature and relative humidity of
 12 the air streams. The measurement of the RH and temperature for both the inlet and outlet air
 13 streams are recorded with sampling intervals of 1 s using calibrated thermocouples and the
 14 humidity sensors. A cyclic generator unit (CGU) that has two linear slide actuators that are
 15 responsible for the movement of the exchanger between the two airstreams. Consequently, the

1 CGU subjects the exchanger to continuous dehumidification (adsorption) and regeneration
 2 (desorption) cycles. This allows for the conversion of the rotation of the wheel to linear motion
 3 and simulates the actual operating conditions of a wheel. A signal-board microcontroller is also
 4 used to control the actuators for various cycle frequencies up to 1 Hz (1000 ms period). Data
 5 acquisition was done using Lab View and experimental uncertainty analysis was done based on
 6 ANSI/ASHRAE Standard 84 recommendation [40]. A detailed description of the test facility has
 7 been reported in previous publications [41,42]

8 **2.3 Single Step change Tests: Theory and Procedure**

9 In this method, latent effectiveness of the small-scale FF exchanger is predicted from its
 10 response to a step change in the inlet humidity. Fathieh et al. [11] developed a double exponential
 11 model (DEM) to predict the characteristic (time constant) of an energy wheel from the normalized
 12 humidity response using Eqs. 1(a) and (b). The time constants and weighing factors are used to
 13 determine the number of transfer units (NTU) and the effectiveness using Eqs. (3) and (4).

$$W(t) = 1 - \gamma_1 e^{\frac{-t}{\tau_1}} - \gamma_2 e^{\frac{-t}{\tau_2}}, \quad 0 \leq t \leq \infty \quad (\text{step increase or adsorption}) \quad 1 \text{ (a)}$$

$$W(t) = \gamma_1 e^{\frac{-t}{\tau_1}} + \gamma_2 e^{\frac{-t}{\tau_2}}, \quad 0 \leq t \leq \infty, \quad (\text{step decrease or desorption}) \quad 1 \text{ (b)}$$

$$\gamma_1 + \gamma_2 = 1, \quad \tau_1, \tau_2 > 0 \quad (2)$$

$$NTU = -\frac{1}{2} \left\{ 1 - \left(\frac{2\omega}{\pi} \right) \gamma_1 \tau_1 \frac{\left(\frac{1 - e^{-\frac{\pi}{\omega\tau_1}}}{1 - e^{-\frac{\pi}{\omega\tau_1}}} \right)^2}{\left(\frac{1 - e^{-\frac{\pi}{\omega\tau_1}}}{1 - e^{-\frac{\pi}{\omega\tau_1}}} \right)} - \left(\frac{2\omega}{\pi} \right) \gamma_2 \tau_2 \frac{\left(\frac{1 - e^{-\frac{\pi}{\omega\tau_2}}}{1 - e^{-\frac{\pi}{\omega\tau_2}}} \right)^2}{\left(\frac{1 - e^{-\frac{\pi}{\omega\tau_2}}}{1 - e^{-\frac{\pi}{\omega\tau_2}}} \right)} \right\} \quad (3)$$

$$\varepsilon_1 = \frac{NTU}{1+NTU} \quad (4)$$

14 where $W(t)$ is the normalized humidity response, ω denotes the wheel angular speed, and τ is the
 15 time constant for wheel response to the step change in inlet humidity. Two-time constants (τ_1
 16 and τ_2) stand for wheel response are attributed to a fast mass transfer mode (for adsorption on
 17 external surfaces and macropores) followed by a slow mode (for adsorption on micropore and
 18 mesopore sites with large diffusion barriers) [17,43]. The weighting factors γ_1 and γ_2 represent
 19 the mass transfer needed factor for these two modes highlighted above.

20 The test conditions used for the performance tests are listed in Table 2. The experimental
 21 procedure involves three steps, namely: pre-conditioning, humidity step change, and single step

1 measurements. During the pre-conditioning step, air streams at a specified temperature and
 2 humidity were passed through the ducts for a minimum of 1 h before the step change to achieve
 3 steady-state conditions. For the dehumidification tests, dry air (RH < 9%) was used for exchanger
 4 pre-conditioning until steady-state conditions was reached. For the humidity step change, the inlet
 5 humidity was changed quickly (< 1 s) by automatically sliding the exchanger rapidly from dry air
 6 stream to humid air stream. For the regeneration tests, after pre-conditioning the exchanger with
 7 humid airflow, the exchanger was slid to dry air stream. As a result, dry air will flow through the
 8 exchanger, and desiccants start desorbing the adsorbed water. In the last step (single step
 9 measurements), the temperature and humidity at the inlet and outlet of the test section were
 10 recorded, until the outlet humidity reached the inlet humidity, and these data denote the single step
 11 response of the exchanger.

12 **Table 2:** Operating Conditions used for both Single Step change and Cyclic Experiments

Q_a (L/min)	V_f (m/s)	Re_{ch}	T_{air} (°C)	RH_{dry} (%)	RH_{humid} (%)	$(\Delta RH)_{step}$ (%)
15 ± 1	0.050 ± 0.001	26 ± 2	23 ± 0.5	7 ± 2	50 ± 2	43 ± 2

13 2.4 Cyclic Tests: Theory and Procedure

14 In cyclic tests, the exchanger was exposed to alternative adsorption and desorption cycles,
 15 and the latent effectiveness is determined from the instantaneous humidity and temperature
 16 measurements at the exchanger inlets and outlets using Eqs. 5 (a) and (b),

$$\varepsilon_{1-ads} = \frac{\dot{m} (W_1 - W_3)}{\dot{m} (W_1 - W_2)} \quad 5 (a)$$

$$\varepsilon_{1-des} = \frac{\dot{m} (W_4 - W_2)}{\dot{m} (W_1 - W_2)} \quad 5 (b)$$

17 where W is the absolute humidity of airstream at the inlets and outlets of the exchanger. Subscripts 1, 2, 3
 18 and 4 indicate the inlets and outlets of humid and dry air streams, respectively. $\dot{m}(W_1 - W_3)$ is the
 19 amount of moisture adsorption rate during the adsorption cycle and $\dot{m} (W_4 - W_2)$ is the moisture
 20 desorption rate during the desorption cycle. ε_{1-ads} and ε_{1-des} are the latent effectiveness of the
 21 adsorption and desorption processes, respectively

1 The exchanger was exposed to a series of sorption cycles until the outlet air streams (air
 2 ducts 3 and 4) reached steady-state conditions. A dynamic steady state is reached by the exchanger
 3 when the difference between the average effectiveness of two cycles is less than 1%, which is
 4 below the uncertainty limit. In these experiments, 120 s was used as the period, which is equal to
 5 0.5 rpm, and the other test conditions are same as specified in Table 2.

6 **2.5 Uncertainty Analysis**

7 The uncertainty in latent effectiveness is estimated from the uncertainties in temperature,
 8 humidity, and flowrate measurements for the cyclic experimental results. For the single step test
 9 results, additional uncertainties in the curve fitting and time constants are included in the analysis.
 10 The uncertainties of the measured variables (temperature, humidity and flow rate) are $\pm 0.2^\circ\text{C}$,
 11 $\pm 1.5\%$, and 2% respectively. The equipment used to measure these parameters are T-type
 12 thermocouples, capacitive type humidity sensor and MKS type 1559A flow controllers. The total
 13 uncertainty (U) in the measurement is determined from the systematic (B_x) and random (P_x)
 14 uncertainties for 95% confidence intervals according to the ASME PTC standard 19.1 [44]:

$$U = \sqrt{P_x^2 + B_x^2} \quad (6)$$

15 The random uncertainty (P_x) is estimated using Eqn. (7)

$$P_x = \frac{t_x \cdot SD}{N} \quad (7)$$

16 where t_x is the student t- factor at a 95% confidence interval for a degree of freedom of (N-1), and
 17 SD is the standard deviation of the measurements. The uncertainty in latent effectiveness is
 18 determined following the rules of uncertainty propagation and using Eqn. (8) below.

$$U_R = \left[\sum_{i=1}^j \left(\frac{\partial R}{\partial p_x} U_{px} \right)^2 \right]^{0.5} \quad (8)$$

19 where U_R , U_{px} , and $\partial R / \partial p_x$ are the overall uncertainty, uncertainty in measurement property p_x
 20 and the sensitivity coefficient of measurement property p_x , respectively.

21 **2.6 Energy Wheel Literature Correlation**

1 The results obtained from the single step change and cyclic experimental tests were used
2 to validate the literature correlation proposed by Simonson and Besant. The correlation (Eqs. (9)-
3 (15)) were previously validated with conventional desiccants such as silica gel and molecular
4 sieves [8]. The latent effectiveness is expressed as a function of the number of transfer unit (NTU),
5 heat capacity rate ratio (Cr^*), maximum moisture content (W_m), average relative humidity (ϕ_{ave}),
6 the slope of sorption isotherm $\left[\frac{\partial u}{\partial \phi}\right]_{\phi_{ave}}$, and the operating condition factor (H^*). The correlations
7 accurately predict the latent effectiveness within $\pm 2.5\%$ for $3 \leq Cr^* \leq 10$ and $2 \leq NTU \leq 10$,
8 $0.1 \leq W_m \leq 0.5$, $0 \leq \eta \leq 0.1$, $-6 \leq H^* \leq 6$, $1 \leq \frac{Cr^*}{Cr_m^*} \leq 5$, $C=1$, and $C^* = 1$ conditions [8].

$$\epsilon_l = \frac{NTU}{1 + NTU} \left[1 - \frac{1}{0.54 (Cr_{mt}^*)^{0.86}} \right] \times \left[1 - \frac{1}{(NTU)^{0.51} (Cr^*)^{0.54} H^*} \right] \quad (9)$$

where, (10)

$$NTU = \frac{1}{\dot{m}c_{p,a}} \left[\frac{1}{(hA_s)_s} + \frac{1}{(hA_s)_e} \right]^{-1} \quad (11)$$

$$Cr^* = \frac{MC_{p,m}N}{\dot{m}c_{p,a}}, \quad 3 \leq Cr^* \leq 10 \quad (12)$$

$$Cr_m^* = \frac{M_{d,dry}N}{\dot{m}_a} \quad (13)$$

$$Cr_{mt}^* = (Cr_m^*)^{0.58} W_m^{0.33} \left(\left[\frac{\partial u}{\partial \phi} \right]_{\phi_{ave}} \right)^{0.2} (Cr^*)^{1.13} \left[\frac{e^{\frac{1482}{T_{ave}}} - 1.26 (\phi_{ave})^{0.5}}{47.9} \right]^{4.66} \quad (14)$$

$$H^* = 2500 \frac{\Delta W}{\Delta T}, \quad -6 \leq H^* \leq 6 \quad (15)$$

9

10 3. DESICCANT TREATMENT

11 3.1 Mechanical Treatment

12 Before coating FF particles onto the Al plates as the desiccant material, the FF was
13 subjected to pre-treatment, which includes ball milling, grinding, and sieving through a mesh size
14 #70 sieve to achieve particle sizes of 210 μm that were used herein.

15 3.2 Water Vapor Adsorption

1 The vapor adsorption analysis of the FF (210 μm) was performed using the Intelligent
2 Gravimetric Analyzer system (IGA-002) supplied by Hiden Isochema Ltd. (Warrington, United
3 Kingdom). The IGA-002 is equipped with a sensitive microbalance with a resolution of 0.1 μg and
4 an uncertainty of $\pm 1 \mu\text{g}$. The sample holder is housed within a stainless-steel reactor to create ultra-
5 high vacuum conditions and eliminate changes in the external environment. For each experiment,
6 ca. 30 - 35 mg of sieved FF was loaded in the stainless-steel sample holder and placed in the reactor
7 chamber. The desired temperature inside the reactor was precisely controlled using a water bath
8 with an accuracy of $\pm 0.1^\circ\text{C}$. Prior to the start of the isotherm measurements, samples were
9 thoroughly degassed and dried at 70°C under vacuum ($\approx 10^{-7}$ mbar) for 6 h and held isothermally
10 at 25°C . The adsorption isotherm measurements were acquired at 25°C for different pressure
11 values over the relative pressure (P/P_0) range of 0 to 1. This process was repeated for FF with
12 different particle sizes (125 and 420 μm) and chemically treated FF (peroxyacetic acid, CHT-1;
13 and chlorite treated, CHT-2). A detailed procedure of the chemical treatment of the FF, and the
14 characterization results are highlighted in previous studies [38,39], as mechanical and chemical
15 treatment is believed to enhance some moisture adsorption properties of FF.

16 **4. RESULTS AND DISCUSSION**

17 The performance results obtained from the test data and correlation are presented in this section.

18 **4.1 Moisture Adsorption Performance Test Results**

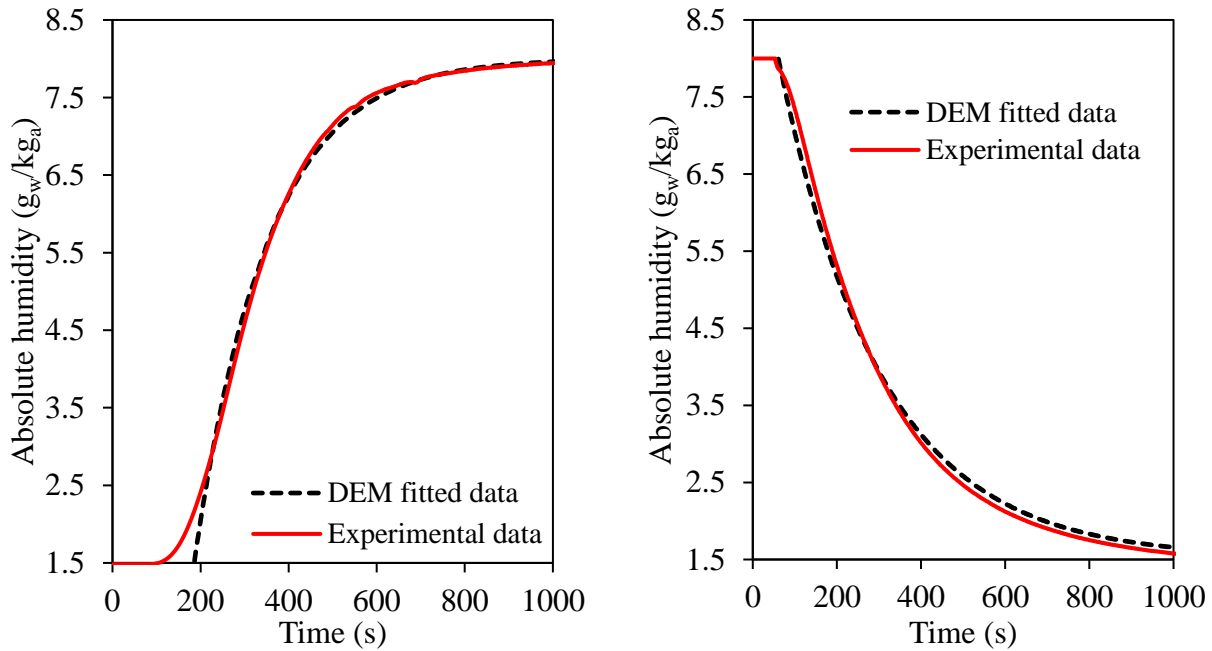
19 **4.1.1 Single step change tests**

20 The humidity response at the outlet of small-scale FF-coated exchanger for both step
21 increase and decrease over time are shown in Figs. 3(a-b). The normalized humidity at the
22 exchanger outlet (Eqn. (16)) was used to calculate the time constants of the exchanger,

$$W(t) = \frac{W_{\text{out},t} - W_{\text{out},t=0}}{W_{\text{out},\text{final}} - W_{\text{out},t=0}} \quad (16)$$

23 where, $W(t)$ is the instantaneous normalized humidity ratio and t is the time. During the adsorption
24 process (Fig. 3(a)), the humidity gradually increased from 1.5 g_w/kg_a to 6.8 g_w/kg_a within the first
25 500 s, which provides an indication that the FF-coated exchanger had reached 85% of its
26 equilibrium moisture during the first 500 s. As the test continues, ca. 800 s, the humidity levels of
27 both supply and exhaust air streams reach a congruent value of 8 g_w/kg , indicating that the

1 desiccant bed is saturated with adsorbed water vapor. An opposite trend was observed during the
 2 desorption process (Fig. 3(b)), with W steadily decreasing from 8 g_w/kg to 2.5 g_w/kg within the
 3 first 500 s of operation, before it decreased to the inlet value after 800 s (no desorption). To
 4 estimate the NTU for moisture and the ε_t of the energy wheel for the single step operation,
 5 experimental data are fitted to DEM. The fitted data for the adsorption process using the double
 6 exponential model (DEM) is shown in Fig. 3(a), along with the measurements from the results of
 7 the adsorption-desorption data shown in Figs. 3(a-b), there is close agreement between the
 8 experimental and fitted data, which is supported by the value of R^2 ($R^2 = 0.998$), obtained from the
 9 data fitting. Other parameters, such as the time constant and weighting factors related to the DEM
 10 are presented in Tables 3.



11 **Figure 3.** Humidity response of FF-coated small-scale exchanger during (a) adsorption and (b)
 12 desorption for single step test.

13 **Table 3:** The exchanger response to time constants and weighing factors obtained for step
 14 change in the inlet humidity ($Re_{dh} = 26$ and $T_{air} = 23$ °C)

$(\Delta RH)_{step}$	$(\Delta RH)_{step}$	γ_1	τ_1 (s)	γ_2	τ_2 (s)	R^2
step increase	50 ± 2	0.79	354.7	0.21	152.0	0.998
step decrease	50 ± 2	0.75	373.3	0.25	148.5	0.998

15

1 The humidity profile presented in Fig. 3 indicates a gradual increase in the humidity of the
2 air at the outlet stream until it reaches the humidity in the inlet. During the adsorption process
3 (when water vapor is adsorbed onto the adsorption sites), the difference in the concentration of
4 water vapor between the air flow and the adsorbent surface is reduced, leading to a decrease in the
5 driving force for mass transfer.

6 **4.1.2 Cyclic tests**

7 The outlet humidity profile of the FF coated exchanger for the cyclic test at angular speed
8 ($\omega = 0.5$ rpm), for both adsorption and desorption cycles are presented in Fig. 4. The profiles were
9 obtained after 1 h of operation when the system had reached a quasi-steady state condition. One
10 complete cycle consists of a half cycle of adsorption and half cycle of the desorption process. From
11 Fig. 4, during the adsorption period, the desiccant adsorbed moisture from the humid air stream as
12 it passes through the exchanger. For the desorption period, FF desiccant releases the adsorbed
13 moisture from the first half cycle to the dry air stream as it passes through the exchanger, making
14 the exit air stream humid.

15 This process continues all through the adsorption-desorption steps of the cyclic test. The value of
16 the humidity during cyclic operation varied between $1.5 \text{ g}_w/\text{kg}_a < W < 8 \text{ g}_w/\text{kg}_a$, as seen in Fig. 4,
17 which is similar to the results for the single step change test. More importantly, based on the
18 humidity profiles, the rate of adsorption and desorption are approximately equal throughout the
19 recorded cycles during the cyclic test after the system reaches a quasi-steady state. This could be
20 an indication that the sorption process takes place at quasi-equilibrium, and all sorption sites of the
21 desiccant were in constant exchange throughout the entire duration of the experiment. It should
22 also be noted that the initial variations (few seconds at the beginning of adsorption and desorption
23 cycles) in normalized humidity is due to the slow response of humidity sensors [45].

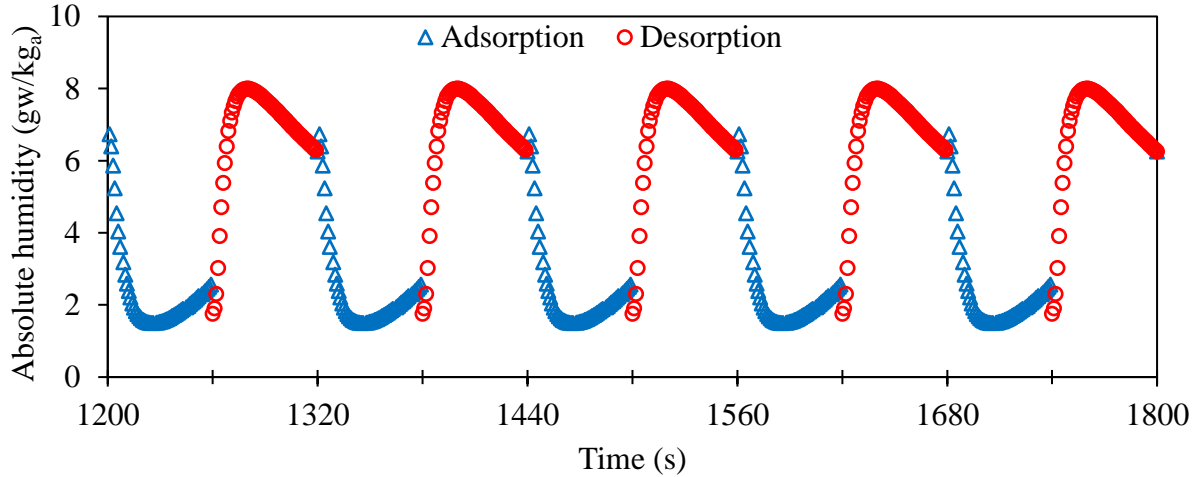


Figure 4. Absolute humidity at the exchanger outlet during adsorption and desorption periods for the FF- coated exchanger during the cyclic test.

1

2 **4.1.3 Comparison of the latent effectiveness (ϵ_l) of the cyclic and single step change tests**

3 The performance of the FF coated exchanger for moisture adsorption was quantified
 4 using ϵ_l . For the single step change tests, the values obtained for the exchanger time constants and
 5 weighting factors (from the adsorption and desorption) data given in Table 3 were substituted into
 6 Eqn. (3) to get the NTU, from which ϵ_l was calculated using Eqn. (4). Since this is a predictive
 7 method, the ϵ_l value for the FF-coated exchanger was estimated at different angular velocity for
 8 both adsorption and desorption cycles at the same NTU condition, where the obtained results are
 9 presented in Fig. 5. The results show an increase in the value of ϵ_l as the wheel angular speed
 10 increases. For a value of angular speed of $0 \leq \omega \leq 20$, the predicted ϵ_l ranges from $76\% \leq \epsilon_l \leq 87\%$
 11 for both adsorption and desorption processes. More importantly, the value of ϵ_l is approximately
 12 equal for both the adsorption and desorption cycles, an indication that the moisture uptake and
 13 removal occurred at a steady state condition.

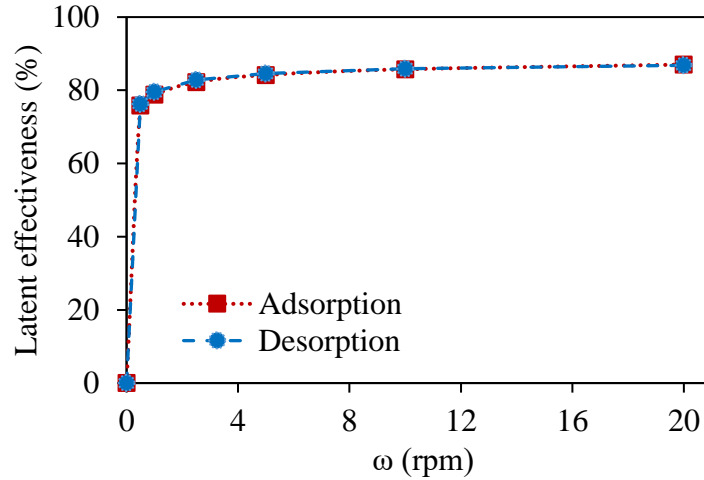


Figure 5. Predicted latent effectiveness of the FF coated exchanger during adsorption and desorption cycles for the single step operation.

1 For the cyclic operation, the value of ϵ_l was estimated for the adsorption and desorption cycle at a
 2 fixed angular speed ($\omega = 0.5$ rpm). The values obtained were compared to those achieved from the
 3 predictive single step method. The effectiveness of the cyclic test at room temperature for five
 4 different adsorption and desorption cycles was determined using Eqs. 5(a) and 5(b), respectively,
 5 as proposed in the ASHRAE standard method [40]. The results obtained are shown in Fig. 6, and
 6 the average ϵ_l (from the five cycles) for both the adsorption and desorption cycles during the
 7 cyclic operation along with the single step test results at (ω) = 0.5 rpm are presented in Table 5.

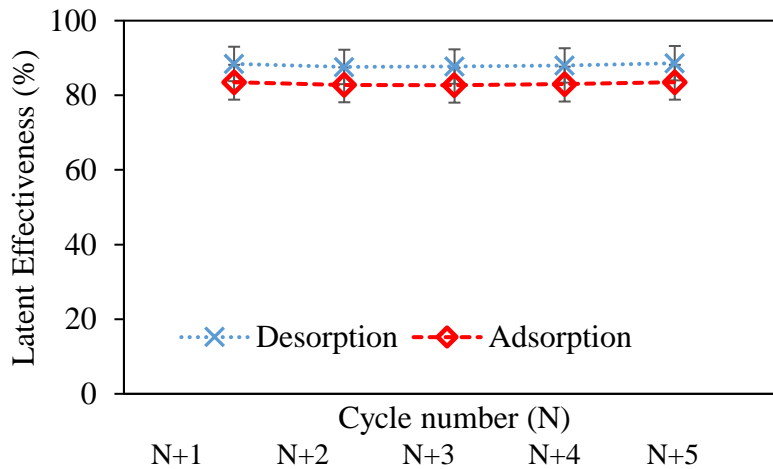


Figure 6. Latent effectiveness of the FF coated exchanger during the adsorption and desorption cycles for the cyclic test after reaching quasi-steady state.

1 **Table 5:** Comparative data of latent effectiveness of the FF coated exchanger for both cyclic and
 2 single step tests.

ω	$\epsilon_{\text{cyclic}} (\%)$		$\epsilon_{\text{single step}} (\%)$		$\epsilon_{\text{cyclic}} - \epsilon_{\text{single step}} (\%)$	
	ϵ_{ads}	ϵ_{des}	ϵ_{ads}	ϵ_{des}	ϵ_{ads}	ϵ_{des}
rpm						
0.5	83	88	76	76	7	12

3

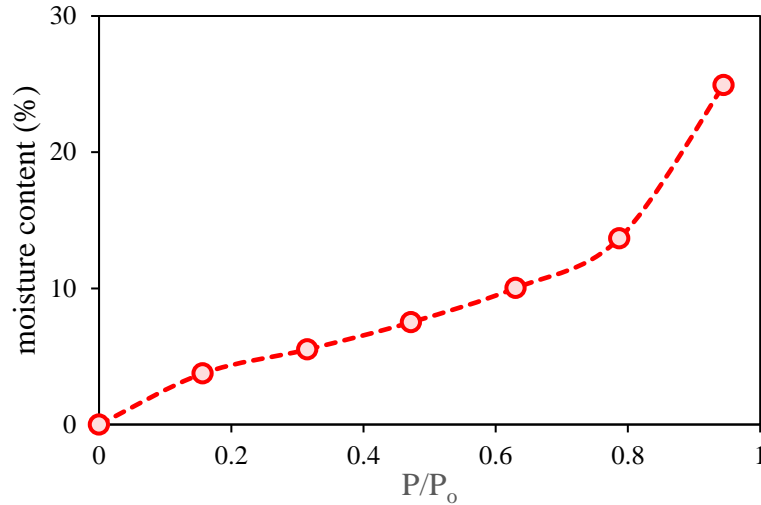
4 The FF- coated exchanger in the cyclic test showed an average ϵ_l value of 86 % for both
 5 adsorption and desorption cycles. Additionally, the latent effectiveness of the desorption cycle (86
 6 %) was found to be slightly higher than the adsorption cycle (83%), as seen in Fig. 6, even though
 7 the difference is still within the range of experimental uncertainty. The uncertainties in latent
 8 effectiveness are near 5%, where this lower value can be attributed to the high accuracy of
 9 instrumentation as indicated in the uncertainty analysis. This level of uncertainty in effectiveness
 10 can also depend on the operating conditions, as a higher difference between the humidity ratios of
 11 two supply airstreams can cause a reduction in the value of uncertainty in latent effectiveness.
 12 Additionally, an accurate control of flow rate and relative humidity can reduce the random
 13 uncertainty in the measured variables. More so, the ASHRAE standard 84 recommends reporting
 14 latent effectiveness to within $\pm 7\%$ uncertainty [46], which facilitated the design of the test facility
 15 and test conditions to give a latent effectiveness value within this acceptable range. Also, a
 16 considerable difference was observed between the values obtained for ϵ_l of the FF coated
 17 exchanger during the cyclic and single step tests, as noted in Table 5. The ϵ_l value of the adsorption
 18 and desorption cycles were found to be approximately the same, while a difference of 7% and 12%
 19 were respectively observed when compared to the effectiveness values of the adsorption-
 20 desorption cycle of the single step and cyclic tests. Overall, approximately 9.5% difference in
 21 average ϵ_l was noticed between the cyclic and single step processes. Since the calculation of the
 22 effectiveness of the single step test is based on a predictive model, a deviation of 9.5 % from the
 23 value obtained for the cyclic test is still within an acceptable uncertainty limit, according to Fathieh
 24 et al. [11]. Thus, there is a good agreement between the effectiveness obtained from the single step
 25 DEM model and the data obtained from the cyclic test.

1 **4.2 Sorption and physio-chemical properties of flax-fiber**

2 **4.2.1 Water vapor adsorption**

3 The result of the water vapor adsorption analysis of FF (particle size 210 μm) is shown in
4 Fig. 7. The moisture content or uptake is presented as a function of relative pressure (P/P_0) is
5 presented, where P/P_0 is the ratio of absolute pressure to the saturation pressure. The results of the
6 chemically treated FF and other particle sizes are presented in the supplementary information (SI;
7 cf. Figs. S1 to S4).

8 Based on IUPAC classification, the isotherm displayed a type II profile, which is
9 characteristic of a macro-porous material with mono-layer adsorption profile [47,48]. It can be
10 seen from the isotherm profile that the sorption capacity increases with the relative pressure, an
11 indication of a strong relationship between the adsorbent porosity and the vapor uptake capacity.
12 At low relative pressure (close to 0.2), the water can be adsorbed on the surface, which concurs
13 with the formation of a monolayer adsorption profile. The formation of bi- or multi-layer
14 adsorption of water is possible as the relative pressure attained a value close to 0.8. Overall, a total
15 water uptake capacity of 25% was reached at a relative pressure of 0.9 for FF. This value is
16 comparable to the values obtained from conventional desiccants such as silica gel, MOFs, and
17 starch reported in the literature [49]. The desiccant adsorption capacity with water can be
18 influenced by the amount of the accessible surface functional groups, the polarity of the bio-
19 adsorbent, and the presence of the amorphous and crystalline domains of the adsorbent [50].
20 Detailed characterization results of FF with respect to the textural properties, morphology,
21 crystallinity, water swelling propensity and their contribution to moisture performance of FF are
22 presented elsewhere [21,38,39].



1

2 **Figure 7:** Equilibrium vapor adsorption-desorption isotherm of FF desiccant at 25 °C. The
 3 dashed line provides a guide to view the trend in moisture content with relative humidity.

4 **4.2.2 Physiochemical properties**

5 The results of the SEM imaging of the FF are shown in Fig. 8. The non-porous strands of FF are
 6 evident in the in the 2D images. Studies have reported that the raw FF materials also consist of
 7 non-cellulosic components such as waxes and oils indicate that such hydrophobic components are
 8 removed during the mechanical treatment. The detailed outline of the characterization results and
 9 comparison between raw FF material and mechanically treated FF is provided elsewhere [38],
 10 [39].

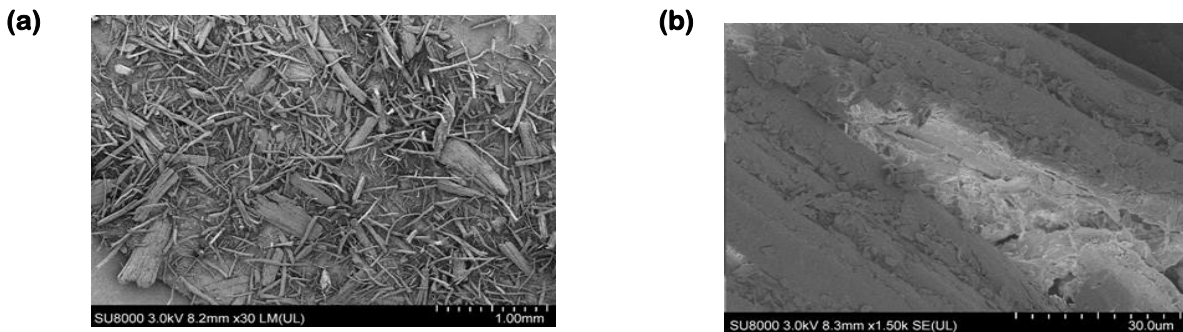


Figure 8. SEM images of flax fiber at two different magnification levels (a) x30 and (b) x1.5K

11 The textural, surface and water vapor uptake properties of flax fiber is reported in Table 6. The
 12 water uptake of the material is 4.26 g_w/g_d and surface area is 1.41 cm^2/g . Though the surface area
 13 of FF is lower than that of conventional desiccant materials, the comparable moisture transfer

1 performance is because of its high-water swelling capacity. These results are supported according
 2 to nitrogen adsorption isotherms and gravimetric swelling tests [38].

3 **Table 6:** Physio-chemical and water vapor uptake properties of flax fiber

Surface Area (cm ² /g) ^a	1.41
Pore Width (nm) ^a	0.95
Pore Volume (cm ³ /g × 10 ⁻²) ^a	3.56 × 10 ⁻¹
Water Swelling (%) ^b	735
Vapor uptake (g/g) ^c	4.92
K _{BET} (L/mol) ^c	178

^aObtained from N₂ adsorption studies; ^bGravimetric water swelling; ^cObtained by fitting vapor adsorption data to the BET equation

4

5 **4.3 Comparison of Latent Effectiveness Obtained from Experiments with Literature** 6 **Correlation**

7 The input parameters for literature correlation, along with their description for the small-
 8 scale exchanger are summarized in Table 7. Using these values in Eqn. (8), the ε_l of the small-
 9 scale exchanger was calculated. Based on the assumption of Simonson and Bessant [8], the Lewis
 10 number is unity, and the NTU values for both heat and mass transfer are the same. The results
 11 obtained from this correlation at different angular speeds are presented in Fig. 9(a), within the
 12 validity range of $3 \leq Cr^* \leq 10$. The ε_l values obtained from the single step change tests are also
 13 included for comparison, while the correlation for single step and cyclic results obtained at $\omega =$
 14 0.5 rpm are shown in Fig. 9(b). The results in Fig. 9(a) show that an increase in ω will lead to
 15 higher latent effectiveness which concurs with literature findings [51–53]. The moisture transfer
 16 rate between the desiccants and air streams has the highest value at the beginning of each
 17 adsorption/desorption cycle. Thus, a shorter cycle period (higher angular speed) will lead to a
 18 higher value of effectiveness. At low angular speeds, the desiccant is exposed to the airstream for
 19 a long duration leading to a lower value of the latent effectiveness. Conventionally, the energy
 20 wheels usually operate at 10-20 rpms for getting maximum latent effectiveness. If the wheel rotates
 21 too fast, the effect of carryover (i.e., cross contamination between the two airstreams may occur

1 due to the high amount of air trapped in the exchanger) will be significant, which is undesirable in
 2 many situations.

3 From the results presented in Fig. 9(b) at $\omega = 0.5$ rpm, a value of 85.7 % predicted by the
 4 correlation (equation (11)) is approximately equal to 85.5% obtained from the cyclic test, as
 5 compared to a value of 76 % for the single step test. Although cyclic testing was not performed at
 6 higher angular speeds, the values given by the single step prediction is close to the one obtained
 7 from the model developed by Simonson and Bessant [8], within the limit of uncertainty stated by
 8 Fathieh et al. [11] for the single step DEM fitting model.

9 **Table 7.** Descriptions and correlation parameters used to determine the latent effectiveness of the
 10 FF coated exchanger.

Parameter	Description	Values	References
h (W/m ² K)	Convective heat transfer coefficient	28 ± 0.5	Ref. [60]
A_s (m ²)	Total area of heat transfer	0.48 ± 0.008	Measured
M (g)	Mass of coated matrix	513	Measured
$C_{p,m}$ (J/kg K)	Specific heat capacity of matrix	893	Al-3003
$M_{d, dry}$ (g)	Total mass of dry desiccant coated on the matrix	11.69	Measured
W_m (g/g)	Maximum moisture content of desiccant	0.25	Fig. 7
ϕ_{ave}	Average relative humidity	0.24	Table 2
$S(\partial u / \partial \phi)_{ave}$	Slope of sorption isothermal average relative humidity	0.14	Fig. 7
H^*	Operating condition factor	$H^* \gg 1$	$\Delta T = 0$

11

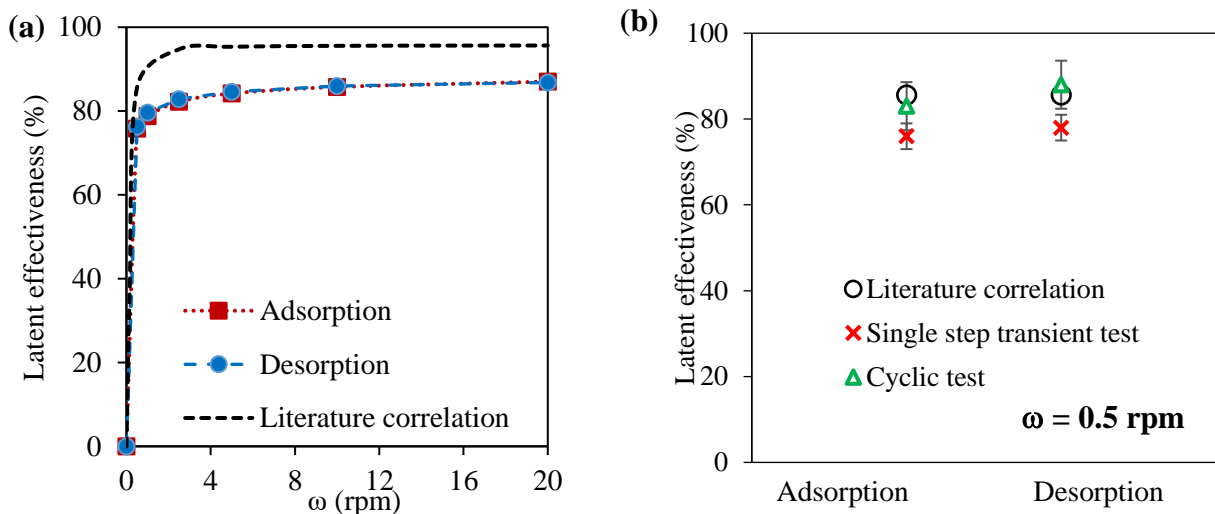


Figure 9. Latent effectiveness at different angular speed from literature correlation during (a) single step change and (b) cyclic tests

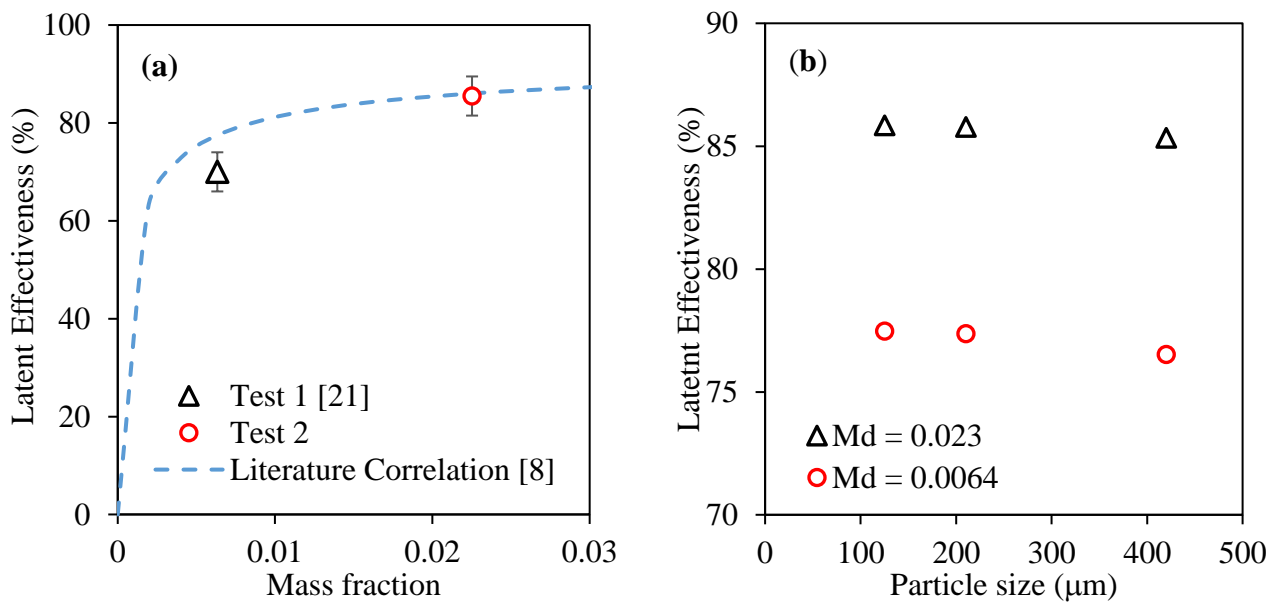
The difference in experimental data and literature correlations can be related to the measurement uncertainties in experiments (ca. 5%) and the range of applicability of correlation proposed by Simonson and Besant [8]. The model proposed a range of $3 < Cr^* < 10$, which was validated numerically for a desiccant with a linear sorption isotherm. However, the isotherm of FFs presented herein are not linear for the entire humidity range, whereas a linear curve has to be fitted to determine the slope of sorption curve within the operating humidity range of the experimental conditions. Other contributing factors may result from simplified assumptions such as equality of the convective mass transfer and the heat transfer coefficients, equality of the area of mass transfer to the heat transfer area, as along with experimental uncertainty and errors in the correlation parameters. It should be noted that the slow response of humidity sensors also causes errors in the estimation of effectiveness [45]. However, the correlated results gave satisfactory agreement with the cyclic test.

4.4 Effect of Particle Size, Desiccant Mass Fraction, and Chemical Treatment on the Moisture performance of FF Desiccant

Different chemical processes have shown to be viable for the conversion of carbon compounds to other useful industrial compounds [54–59], and chemical modification of organic carbon compound such as FF has yielded improvements to the moisture ability of the material [39]. Thus, these results quantify the effects of particle size, and chemical treatments on the latent

1 effectiveness of FF-coated energy wheels for HVAC application and represent a noteworthy
2 contribution to the field of bio-desiccant coatings.

3 Fig. 10(a) presents the measured and predicted effectiveness as a function of the mass
4 fraction (M_d) of FF for a particle size of $210\ \mu\text{m}$ and at a wheel speed ($\omega = 0.5\ \text{rpm}$). It should be
5 noted that the desiccant mass fraction is defined as the ratio of mass of desiccant to the total mass
6 of the exchanger. From Fig. 10(a), an increase in effectiveness was observed as the mass fraction
7 of desiccant increases. Beyond 0.02 mass fraction, there was no significant changes in
8 effectiveness with an increase in the mass fraction of desiccant. More so, there was good agreement
9 between the correlation and the experimental data. Thus, within the range of desiccant mass
10 fraction considered herein, an increase in desiccant mass fraction increases the moisture adsorption
11 performance (effectiveness) of FF for potential energy wheel applications.



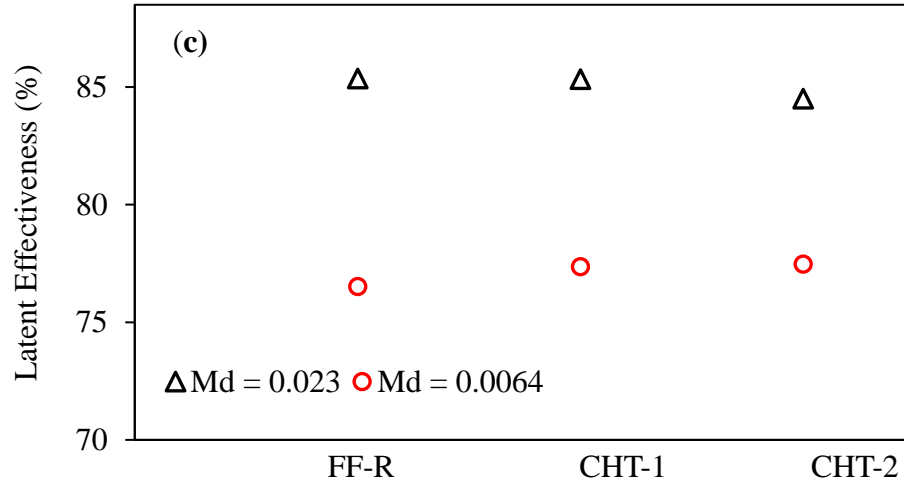


Figure 10: (a) Effect of desiccant mass fraction, (b) particle size, and (c) chemical treatments on latent effectiveness of FF coated small-scale exchanger for two mass loadings of desiccant coating.

1 The predicted effect of particle size and chemical treatments on the effectiveness for the
2 two different desiccant mass fractions ($M_d = 0.0064$ and 0.023) are shown in Figs. 10(b) and (c).
3 No significant differences were observed in the effectiveness of the energy wheel for the three
4 different particle sizes (125, 210, and 420 μm) and chemical treatments. However, the
5 effectiveness is higher for the higher mass fraction of desiccant. Although different
6 characterization techniques have shown improvement in the structural properties and water uptake
7 capacity of the chemically treated FF along with of particle sizes [38,39], the corresponding
8 improvements are not sufficient enough distinguish this effect for moisture performance study in
9 an energy wheel. Note that the moisture adsorption isotherms for the different particle sizes, and
10 chemically treated FF are presented in Figs. S1-S4 (cf. Supplementary information). The isotherms
11 are required to determine W_m (g/g) and $(\partial u / \partial \phi)_{\text{ave}}$ in Eqn. (14).

12 For industrial applications, rotary wheels are usually operated at a speed of 20 rpm, and
13 the desiccant mass fraction is between 0.2 - 0.3. Since we could not carry out tests at higher wheel
14 speeds ($\omega = 20$ rpm), the correlation was used to predict the effectiveness at this speed. Results
15 (Fig. 9(a)) showed that the effectiveness increase with greater wheel speed and attained a value of
16 95 % at 20 rpm. The mass fraction of the desiccant presented herein is lower because of the high
17 weight of the aluminum plates used in the exchanger. If aluminum foil is used instead of plates,
18 the mass fraction of desiccant herein will be between 0.22-0.3, which will be a good representation

1 of the range of typical industrial conditions. Thus, FF has a good desiccant potential for energy
 2 wheel application.

3 **4.5 Comparison of Latent Effectiveness of Commercially Available Energy Wheels with Bio-** 4 **Desiccant Coated Wheels**

5 Some key advantages of biomaterials include their environmental friendly nature,
 6 relatively low material cost, renewable abundance and biodegradability. Previous studies have
 7 shown that biomaterials are cost effective and feasible for energy recovery and drying applications,
 8 as compared with conventional industrial desiccant materials [33]. In this section, the latent
 9 effectiveness of bio-desiccants is compared with that of commercially available desiccants. The
 10 flax fiber (FF) and starch particles (SP) [22] are the biomaterials selected for this study, and ion
 11 exchange resin (modified with magnesium) [60], molecular sieve and silica gel [61] are among the
 12 commercial desiccants considered for the comparison. The sorption profiles of all materials except
 13 FF are used from previously published studies, where the energy wheel correlation is used for ϵ_1
 14 comparison. The mass fraction of desiccants considered for this analysis (M_d) is 0.2.

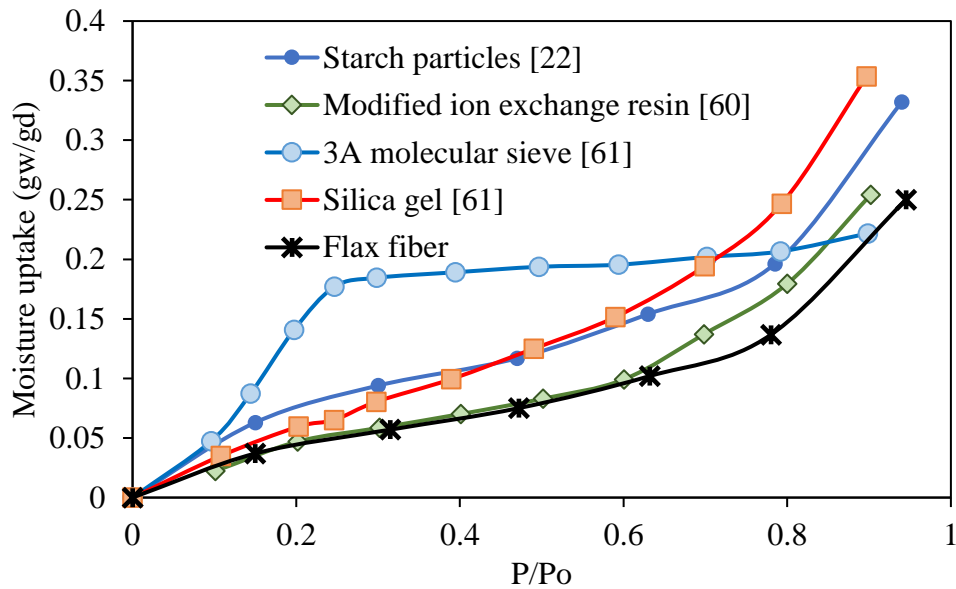


Figure 11: Sorption isotherms of available commercial desiccants and biomaterials.

15 Figure 11 shows the sorption profiles of selected materials reproduced from refs [60,61],
 16 where it is evident that silica gel has the highest moisture uptake and slope $(\partial u / \partial \phi)_{ave}$ among the
 17 various desiccant coatings. The latent effectiveness of energy wheels coated with the selected

1 desiccants are predicted and shown in Fig. 12 for two different NTU conditions. The temperature
 2 of inlet airstreams is assumed to be similar (24 °C) for the relative humidity of 30% and 60%,
 3 respectively. For an NTU of 2.5, the effectiveness varies from 50% to 70% (Cr^* varies from 1-6)
 4 for all the desiccants except molecular sieve. At low Cr^* conditions, silica gel has the highest latent
 5 effectiveness followed by the starch particles, ion exchange resin, flax fibers and molecular sieves
 6 for the operating conditions analyzed. The starch particles perform very similar to silica gel and
 7 their effectiveness is very close within $\pm 0.25\%$. From this analysis, the bio-desiccants are shown
 8 to display a latent effectiveness similar to that of commercial desiccants. However further studies
 9 are needed to evaluate the long-term performance and ageing behavior of bio-desiccants.

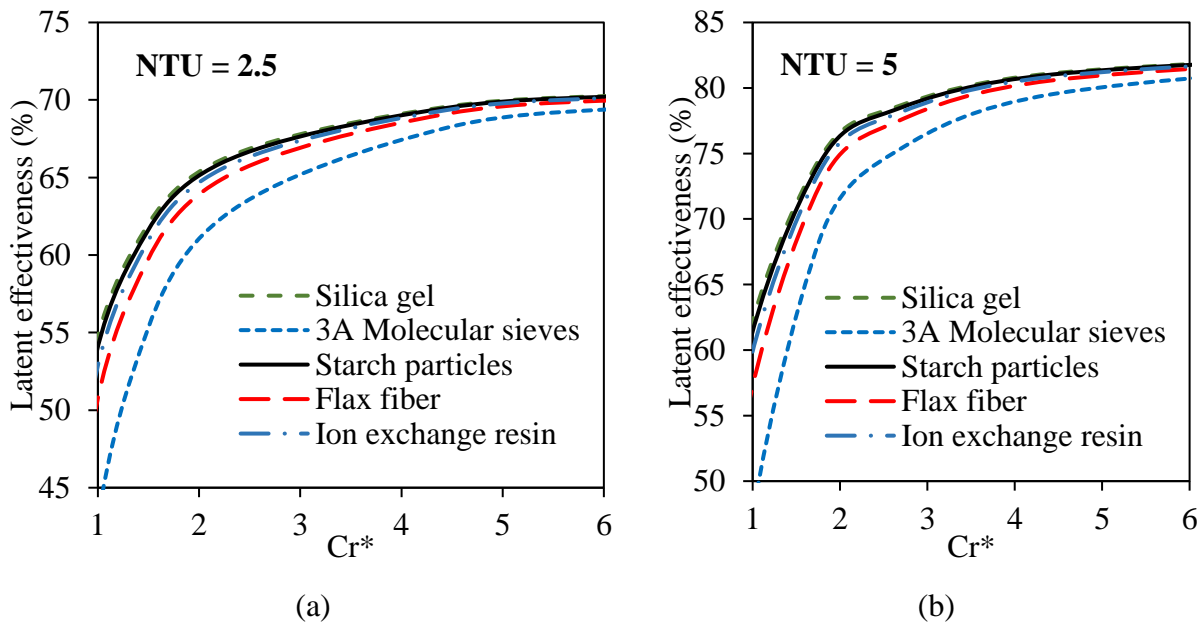


Figure 12: Comparison of latent effectiveness of various commercial desiccants and bio-materials coated energy wheels for (a) NTU= 2.5 and (b) NTU= 5

10

11 5. CONCLUSIONS

12 The latent effectiveness of a Flax Fiber (FF) desiccant coated energy wheel was evaluated from
 13 single-step change and cyclic tests on a FF coated exchanger using a small-scale test facility. The
 14 experimental results were compared with an established energy wheel correlation from the
 15 literature. The major findings from the experiments are summarized below.

- 1 1. The latent effectiveness (of the FF-coated exchanger) obtained from the single step change
2 tests and cyclic tests are in good agreement with the literature correlation within the
3 experimental uncertainty limits.
- 4 2. The desiccant mass fraction has a significant effect on moisture transfer performance
5 (latent effectiveness) of the FF-coated exchanger, while particle size and chemical
6 treatment does not have a significant apparent effect on performance.
- 7 3. The latent effectiveness of various commercially available desiccants and bio-desiccants
8 are predicted using a literature correlation. An energy wheel that uses bio-desiccants would
9 have nearly the same performance as a wheel with commercial desiccants. At $NTU = 5$ and
10 $Cr^* = 2.7$, the latent effectiveness for the various desiccants are: $\epsilon_1 = 78.6\%$ for silica gel,
11 $\epsilon_1 = 78.4\%$ for starch particles, $\epsilon_1 = 78\%$ for ion exchange resin, $\epsilon_1 = 77.5\%$ flax fiber and
12 $\epsilon_1 = 75.2\%$ for molecular sieves.

13 Based on these findings, it can be concluded that biomaterials such as flax-fiber or starch particles
14 can be considered as potential desiccant candidates for energy wheels for HVAC applications with
15 improved sustainability.

16 **ACKNOWLEDGEMENTS**

17 The authors appreciate the financial support of the Government of the Saskatchewan (Ministry of
18 Agriculture) through the Agricultural Development Fund (Project #20160266). Sincere
19 appreciations to Mr. Hayden Reitenbach and Mr. Shawn Reinink (Staff of the Department of
20 Mechanical Engineering) for their technical support in equipment modification and maintenance.

21 **REFERENCES**

- 22 [1] United States Environmental Protection Agency, Indoor Air Quality (IAQ), (2017).
23 <https://www.epa.gov/indoor-air-quality-iaq/introduction-indoor-air-quality> (accessed
24 October 15, 2020).
- 25 [2] Healthlink BC, Indoor Air Quality, (2018). [https://www.healthlinkbc.ca/healthlinkbc-
26 files/indoor-air-quality](https://www.healthlinkbc.ca/healthlinkbc-files/indoor-air-quality) (accessed October 15, 2020).
- 27 [3] ANSI/ASHRAE, Standard 55: Thermal Eenvironmental conditions for human occupancy,
28 Atlanta, GA, 2017.
- 29 [4] Natural Resources Canada, HVAC & Energy Systems, (2020).

- 1 <https://www.nrcan.gc.ca/energy/efficiency/data-research-and-insights-energy-efficiency>
2 (accessed July 4, 2020).
- 3 [5] K.W. Roth, D. Westphalen, J. Dieckmann, S. Hamilton, D. Goetzler, Energy consumption
4 characteristics of commercialbuilding HVAC systems volume III: energy savings
5 potential, 2002.
- 6 [6] W. Goetzler, R. Zogg, J. Young, J. Schmidt, Energy Savings Potential and Research,
7 Development, & Demonstration Opportunities for Residential Building Heating,
8 Ventilation, and Air Conditioning Systems, 2012.
- 9 [7] C.J. Simonson, R.W. Besant, Heat and moisture transfer in energy wheels during sorption,
10 condensation, and frosting conditions, *Journal of Heat Transfer*. 120 (1998) 699–708.
11 <https://doi.org/10.1115/1.2824339>.
- 12 [8] C.J. Simonson, R.W. Besant, Energy wheel effectiveness: part II—correlations,
13 *International Journal of Heat and Mass Transfer*. 42 (1999) 2171–2185.
14 [https://doi.org/10.1016/S0017-9310\(98\)00327-5](https://doi.org/10.1016/S0017-9310(98)00327-5).
- 15 [9] C.J. Simonson, R.W. Besant, Heat and Moisture Transfer in Desiccant Coated Rotary
16 Energy Exchangers : Part I Numerical Model, *HVAC&R Research*. 3 (1997) 325–350.
17 <https://doi.org/10.1080/10789669.1997.10391382>.
- 18 [10] F. Fathieh, M. Nezakat, R.W. Evitts, C.J. Simonson, Effects of physical and sorption
19 properties of desiccant coating on performance of energy wheels, *Journal of Heat*
20 *Transfer*. 139 (2017) 062601. <https://doi.org/10.1115/1.4035650>.
- 21 [11] F. Fathieh, M. Rafati Nasr, S. Sadeh, R.W. Besant, R.W. Evitts, J. Müller, C.J. Simonson,
22 Determination of air-to-air energy wheels latent effectiveness using humidity step test
23 data, *International Journal of Heat and Mass Transfer*. 103 (2016) 501–515.
24 <https://doi.org/10.1016/J.IJHEATMASSTRANSFER.2016.07.046>.
- 25 [12] J.W. Jeong, S.A. Mumma, Practical thermal performance correlations for molecular sieve
26 and silica gel loaded enthalpy wheels, *Applied Thermal Engineering*. 25 (2005) 719–740.
27 <https://doi.org/10.1016/j.applthermaleng.2004.07.018>.
- 28 [13] O.O. Abe, R.W. Besant, C.J. Simonson, W. Shang, Relationship between energy wheel
29 speed and effectiveness and its transient response, part I: Mathematical development of
30 the characteristic time constants and their relationship with effectiveness, in: *ASHRAE*
31 *Transactions*, 2006: pp. 89–102.

- 1 [14] O.O. Abe, Y.H. Wang, C.J. Simonson, R.W. Besant, W. Shang, Transient temperature
2 measurements and characteristics for temperature sensors and energy wheels, in:
3 ASHRAE Transactions, 2006: pp. 76–89.
- 4 [15] W. Shang, R.W. Besant, Theoretical and experimental methods for the sensible
5 effectiveness of Air-to-Air energy recovery wheels, HVAC and R Research. 14 (2008)
6 373–396. <https://doi.org/10.1080/10789669.2008.10391015>.
- 7 [16] W. Shang, R.W. Besant, Effects of pore size variations on regenerative wheel
8 performance, Journal of Engineering for Gas Turbines and Power. 127 (2005) 121–135.
9 <https://doi.org/10.1115/1.1804539>.
- 10 [17] F. Fathieh, A Novel transient testing method for heat/energy wheel components,
11 University of Saskatchewan, Saskatoon, 2016.
12 <https://harvest.usask.ca/handle/10388/7381>.
- 13 [18] F. Fathieh, R.W. Besant, R.W. Evitts, C.J. Simonson, Determination of air-to-air heat
14 wheel sensible effectiveness using temperature step change data, International Journal of
15 Heat and Mass Transfer. 87 (2015) 312–326.
16 <https://doi.org/10.1016/j.ijheatmasstransfer.2015.04.028>.
- 17 [19] M. Shakouri, E.N. Krishnan, L. Dehabadi, A.H. Karoyo, C.J. Simonson, L.D. Wilson,
18 Vapor adsorption transient test facility for dehumidification and desorption studies,
19 International Journal of Technology. 9 (2018) 1092–1102.
20 <https://doi.org/https://doi.org/10.14716/ijtech.v9i6.230>.
- 21 [20] M. Shakouri, E.N. Krishnan, A.H. Karoyo, L. Dehabadi, L.D. Wilson, C.J. Simonson,
22 Water vapor adsorption–desorption behavior of surfactant-coated starch particles for
23 commercial energy wheels, ACS Omega. 4 (2019) 14378–14389.
24 <https://doi.org/10.1021/acsomega.9b00755>.
- 25 [21] W.O. Alabi, A.H. Karoyo, E.N. Krishnan, L. Dehabadi, L.D. Wilson, C.J. Simonson,
26 Comparison of the moisture adsorption properties of starch particles and flax fiber
27 coatings for energy wheel applications, ACS Omega. 5 (2020) 9529–9539.
28 <https://doi.org/10.1021/acsomega.0c00762>.
- 29 [22] M.A. Hossain, A.H. Karoyo, L. Dehabadi, F. Fathieh, C.J. Simonson, L.D. Wilson, Starch
30 particles, energy harvesting, and the “goldilocks Effect,” ACS Omega. 3 (2018) 3796–
31 3803. <https://doi.org/10.1021/acsomega.8b00131>.

- 1 [23] M. Jagirdar, P.S. Lee, J.T. Padding, Performance of an internally cooled and heated
2 desiccant-coated heat and mass exchanger: Effectiveness criteria and design methodology,
3 *Applied Thermal Engineering*. 188 (2021) 116593.
4 <https://doi.org/10.1016/j.applthermaleng.2021.116593>.
- 5 [24] K. Sen Chang, M.T. Chen, T.W. Chung, Effects of the thickness and particle size of silica
6 gel on the heat and mass transfer performance of a silica gel-coated bed for air-
7 conditioning adsorption systems, *Applied Thermal Engineering*. 25 (2005) 2330–2340.
8 <https://doi.org/10.1016/j.applthermaleng.2004.12.020>.
- 9 [25] M. Tatlier, Theoretical investigation of performances of zeolite Y and SAPO-34 coatings
10 for adsorption heat pump applications, *Heat and Mass Transfer/Waerme- Und*
11 *Stoffuebertragung*. 57 (2021) 975–984. <https://doi.org/10.1007/s00231-020-03003-8>.
- 12 [26] X. Zheng, Q. Ma, J. Tan, B. Yu, Preparation and application of UiO-66 in desiccant-
13 coated heat exchanger-based desiccant cooling systems, *Industrial and Engineering*
14 *Chemistry Research*. 60 (2021) 4727–4734. <https://doi.org/10.1021/acs.iecr.1c00077>.
- 15 [27] W. Wang, L. Wu, Z. Li, Y. Fang, J. Ding, J. Xiao, An Overview of adsorbents in the
16 rotary desiccant dehumidifier for air dehumidification, *Drying Technology*. 31 (2013)
17 1334–1345. <https://doi.org/10.1080/07373937.2013.792094>.
- 18 [28] C.H. Chen, P.C. Huang, T.H. Yang, Y.C. Chiang, S.L. Chen, Polymer/alumina composite
19 desiccant combined with periodic total heat exchangers for air-conditioning systems,
20 *International Journal of Refrigeration*. 67 (2016) 10–21.
21 <https://doi.org/10.1016/j.ijrefrig.2016.01.003>.
- 22 [29] W.R. Abd-Elrahman, A.M. Hamed, S.H. El-Emam, M.M. Awad, Experimental
23 investigation on the performance of radial flow desiccant bed using activated alumina,
24 *Applied Thermal Engineering*. 31 (2011) 2709–2715.
25 <https://doi.org/10.1016/j.applthermaleng.2011.04.041>.
- 26 [30] P. Vivekh, M. Kumja, D.T. Bui, K.J. Chua, Recent developments in solid desiccant coated
27 heat exchangers – A review, *Applied Energy*. 229 (2018) 778–803.
28 <https://doi.org/10.1016/J.APENERGY.2018.08.041>.
- 29 [31] Z. Li, S. Michiyuki, F. Takeshi, Experimental study on heat and mass transfer
30 characteristics for a desiccant-coated fin-tube heat exchanger, *International Journal of*
31 *Heat and Mass Transfer*. 89 (2015) 641–651.

- 1 <https://doi.org/10.1016/j.ijheatmasstransfer.2015.05.095>.
- 2 [32] C. Wang, X. Ji, B. Yang, R. Zhang, D. Yang, Study on heat transfer and dehumidification
3 performance of desiccant coated microchannel heat exchanger, *Applied Thermal*
4 *Engineering*. 192 (2021). <https://doi.org/10.1016/j.applthermaleng.2021.116913>.
- 5 [33] J. Khedari, R. Rawangkul, W. Chimchavee, J. Hirunlabh, A. Watanasungsit, Feasibility
6 study of using agriculture waste as desiccant for air conditioning system, *Renewable*
7 *Energy*. 28 (2003) 1617–1628. [https://doi.org/10.1016/S0960-1481\(03\)00003-X](https://doi.org/10.1016/S0960-1481(03)00003-X).
- 8 [34] K.E. Beery, M.R. Ladisch, Chemistry and properties of starch based desiccants., *Enzyme*
9 *and Microbial Technology*. 28 (2001) 573–581. [https://doi.org/10.1016/s0141-](https://doi.org/10.1016/s0141-0229(00)00345-8)
10 [0229\(00\)00345-8](https://doi.org/10.1016/s0141-0229(00)00345-8).
- 11 [35] N. Asim, M.H. Amin, M.A. Alghoul, M. Badiei, M. Mohammad, S.S. Gasaymeh, N.
12 Amin, K. Sopian, Key factors of desiccant-based cooling systems: Materials, *Applied*
13 *Thermal Engineering*. 159 (2019) 113946.
14 <https://doi.org/10.1016/j.applthermaleng.2019.113946>.
- 15 [36] L. Dehabadi, F. Fathieh, L.D. Wilson, R.W. Evitts, C.J. Simonson, Study of
16 dehumidification and regeneration in a starch coated energy wheel, *ACS Sustainable*
17 *Chemistry and Engineering*. 5 (2017) 221–231.
18 <https://doi.org/10.1021/acssuschemeng.6b01296>.
- 19 [37] F. Fathieh, L. Dehabadi, L.D. Wilson, R.W. Besant, R.W. Evitts, C.J. Simonson, Sorption
20 study of a starch biopolymer as an alternative desiccant for energy wheels, *ACS*
21 *Sustainable Chemistry & Engineering*. 4 (2016) 1262–1273.
22 <https://doi.org/10.1021/acssuschemeng.5b01301>.
- 23 [38] A.H. Karoyo, L. Dehabadi, W. Alabi, C.J. Simonson, L.D. Wilson, Hydration and
24 sorption properties of raw and milled flax fibers, *ACS Omega*. 5 (2020) 6113–6121.
25 <https://doi.org/10.1021/acsomega.0c00100>.
- 26 [39] L. Dehabadi, A.H. Karoyo, M. Soleimani, W.O. Alabi, C.J. Simonson, L.D. Wilson, Flax
27 biomass conversion via controlled oxidation: Facile tuning of physicochemical properties,
28 *Bioengineering*. 7 (2020) 1–18. <https://doi.org/10.3390/bioengineering7020038>.
- 29 [40] ANSI/ASHRAE, Standard 84, Method of testing air-to-air heat/energy exchangers,
30 Atlanta, 2020.
- 31 [41] E.N. Krishnan, H. Ramin, A. Gurubalan, C.J. Simonson, Experimental methods to

- 1 determine the performance of desiccant coated fixed-bed regenerators (FBRs),
2 International Journal of Heat and Mass Transfer. (2021).
- 3 [42] E.N. Krishnan, H. Ramin, C.J. Simonson, Performance testing of fixed-bed regenerators
4 for HVAC applications, in: Proceedings of the 2nd Pacific Rim Thermal Engineering
5 Conference, Hawaii, United States, 2019: pp. 1–5.
- 6 [43] Y. Wang, C.J. Simonson, R.W. Besant, W. Shang, Transient humidity measurements: Part
7 I - Sensor calibration and characteristics, IEEE Transactions on Instrumentation and
8 Measurement. 56 (2007) 1074–1079. <https://doi.org/10.1109/TIM.2007.894881>.
- 9 [44] R.S. Figliola; D.E. Beasley, Theory and Design for Mechanical Measurements, 4th ed.,
10 John Wiley & Sons Inc, Hoboken, New Jersey, 2006.
- 11 [45] E.N. Krishnan, H. Ramin, A. Gurubalan, C.J. Simonson, Experimental methods to
12 determine the performance of desiccant coated fixed-bed regenerators (FBRs),
13 International Journal of Heat and Mass Transfer. 182 (2022) 121909.
14 <https://doi.org/10.1016/j.ijheatmasstransfer.2021.121909>.
- 15 [46] ASHRAE, ASHRAE Handbook-HVAC Systems and Equipment, Atlanta, 2020.
- 16 [47] P. Kumar, K.-H. Kim, E.E. Kwon, J.E. Szulejko, Metal–organic frameworks for the
17 control and management of air quality: advances and future direction, Journal of Materials
18 Chemistry A. 4 (2016) 345–361. <https://doi.org/10.1039/C5TA07068F>.
- 19 [48] N.C. Burch, H. Jasuja, K.S. Walton, Water stability and adsorption in metal–organic
20 frameworks, Chemical Reviews. 114 (2014) 10575–10612.
21 <https://doi.org/10.1021/cr5002589>.
- 22 [49] H. Furukawa, F. Gándara, Y.B. Zhang, J. Jiang, W.L. Queen, M.R. Hudson, O.M. Yaghi,
23 Water adsorption in porous metal-organic frameworks and related materials, Journal of the
24 American Chemical Society. 136 (2014) 4369–4381. <https://doi.org/10.1021/ja500330a>.
- 25 [50] T.A. Shittu, F. Idowu-Adebayo, I.I. Adedokun, O. Alade, Water vapor adsorption
26 characteristics of starch–albumen powder and rheological behavior of its paste, Nigerian
27 Food Journal. 33 (2015) 90–96. <https://doi.org/10.1016/j.nifoj.2015.04.014>.
- 28 [51] G. Angrisani, A. Capozzoli, F. Minichiello, C. Roselli, M. Sasso, Desiccant wheel
29 regenerated by thermal energy from a microcogenerator: Experimental assessment of the
30 performances, Applied Energy. 88 (2011) 1354–1365.
31 <https://doi.org/https://doi.org/10.1016/j.apenergy.2010.09.025>.

- 1 [52] U. Eicker, U. Schürger, M. Köhler, T. Ge, Y. Dai, H. Li, R. Wang, Experimental
2 investigations on desiccant wheels, Applied Thermal Engineering. 42 (2012) 71–80.
3 <https://doi.org/10.1016/j.applthermaleng.2012.03.005>.
- 4 [53] N. Enteria, H. Yoshino, A. Satake, A. Mochida, R. Takaki, R. Yoshie, T. Mitamura, S.
5 Baba, Experimental heat and mass transfer of the separated and coupled rotating desiccant
6 wheel and heat wheel, Experimental Thermal and Fluid Science. 34 (2010) 603–615.
7 <https://doi.org/10.1016/j.expthermflusci.2009.12.001>.
- 8 [54] W.O. Alabi, A study of structural properties and performance of Ni-Co-Mg-Al-Ox
9 catalyst for carbon dioxide reforming of methane, University of Saskatchewan, 2018.
- 10 [55] W.O. Alabi, H. Wang, B.M. Adesanmi, M. Shakouri, Y. Hu, Support composition effect
11 on the structures, metallic sites formation, and performance of Ni-Co-Mg-Al-O composite
12 for CO₂ reforming of CH₄, Journal of CO₂ Utilization. 43 (2021) 101355.
13 <https://doi.org/10.1016/j.jcou.2020.101355>.
- 14 [56] W.O. Alabi, CO₂ reforming of CH₄ on Ni-Al-Ox catalyst using pure and coal gas feeds:
15 Synergetic effect of CoO and MgO in mitigating carbon deposition, Environmental
16 Pollution. 242 (2018) 1566–1576. <https://doi.org/10.1016/j.envpol.2018.07.127>.
- 17 [57] W.O. Alabi, K.O. Sulaiman, H. Wang, Sensitivity of the properties and performance of Co
18 catalyst to the nature of support for CO₂ reforming of CH₄, Chemical Engineering
19 Journal. 390 (2020) 124486. <https://doi.org/10.1016/j.cej.2020.124486>.
- 20 [58] W.O. Alabi, K.O. Sulaiman, H. Wang, Y. Hu, C. Patzig, Effect of spinel inversion and
21 metal-support interaction on the site activity of Mg-Al-Ox supported Co catalyst for CO₂
22 reforming of CH₄, Journal of CO₂ Utilization. 37 (2020) 180–187.
23 <https://doi.org/10.1016/j.jcou.2019.12.006>.
- 24 [59] W.O. Alabi, H. Wang, W. Huang, X. Li, A study of CO₂ reforming of CH₄ for coal
25 delivered gases over Ni-based catalysts, Catalysis Today. 309 (2018) 77–82.
26 <https://doi.org/10.1016/j.cattod.2017.10.008>.
- 27 [60] Y. Fang, S. Zuo, X. Liang, Y. Cao, X. Gao, Z. Zhang, Preparation and performance of
28 desiccant coating with modified ion exchange resin on finned tube heat exchanger,
29 Applied Thermal Engineering. 93 (2016) 36–42.
30 <https://doi.org/https://doi.org/10.1016/j.applthermaleng.2015.09.044>.
- 31 [61] X. Zheng, T.S. Ge, R.Z. Wang, Recent progress on desiccant materials for solid desiccant

- 1 cooling systems, *Energy*. 74 (2014) 280–294.
- 2 <https://doi.org/https://doi.org/10.1016/j.energy.2014.07.027>.
- 3